Volume 15
Number 28
28 July 2024
Pages 10673–11150

# Chemical Science

rsc.li/chemical-science

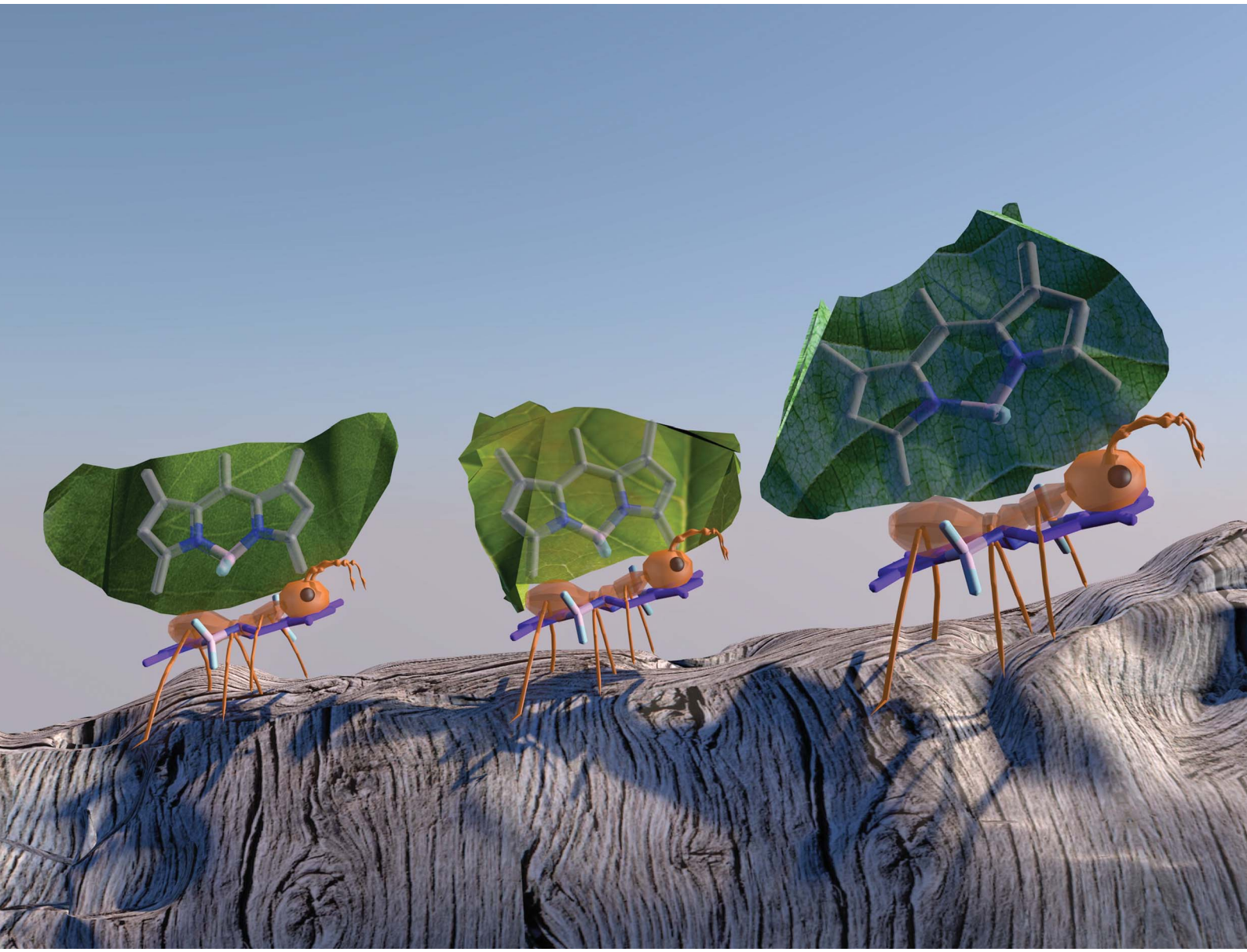

ISSN 2041-6539

ROYAL SOCIETY OF CHEMISTRY

**EDGE ARTICLE**

Gustavo Fernández *et al.*

Pathway-dependent supramolecular polymerization by planarity breaking

Chemical Science

ROYAL SOCIETY OF CHEMISTRY

EDGE ARTICLE

View Article Online
View Journal | View Issue



Cite this: *Chem. Sci.*, 2024, **15**, 10745

All publication charges for this article have been paid for by the Royal Society of Chemistry



# Pathway-dependent supramolecular polymerization by planarity breaking†

Rasitha Manha Veedu, Zulema Fernández, Nils Bäumer, Antonia Albers and Gustavo Fernández *

In controlled supramolecular polymerization, planar π-conjugated scaffolds are commonly used to predictably regulate stacking interactions, with various assembly pathways arising from competing interactions involving side groups. However, the extent to which the nature of the chromophore itself (planar *vs.* non-planar) affects pathway complexity requires clarification. To address this question, we herein designed a new BOPHY dye **2**, where two oppositely oriented $BF_2$ groups induce a disruption of planarity, and compared its supramolecular polymerization in non-polar media with that of a previously reported planar BODIPY **1** bearing identical substituents. The slightly non-planar structure of the BOPHY dye **2**, as evident in previously reported X-ray structures, together with the additional out-of-plane $BF_2$ group, allow for more diverse stacking possibilities leading to two fiber-like assemblies (kinetic **2A** and thermodynamic **2B**), in contrast to the single assembly previously observed for BODIPY **1**. The impact of the less rigid, preorganized BOPHY core compared to the planar BODIPY counterpart is also reflected in the stronger tendency of the former to form anisotropic assemblies as a result of more favorable hydrogen bonding arrays. The structural versatility of the BOPHY core ultimately enables two stable packing arrangements: a kinetically controlled antiparallel face-to-face stacking (**2A**), and a thermodynamically controlled parallel slipped packing (**2B**) stabilized by ($BF_2$) F···H (*meso*) interactions. Our findings underscore the significance of planarity breaking and out-of-plane substituents on chromophores as design elements in controlled supramolecular polymerization.

Received 15th April 2024
Accepted 4th June 2024

DOI: 10.1039/d4sc02499k

rsc.li/chemical-science

## Introduction

Self-assembled structures of π-conjugated chromophores have received considerable interest in recent decades due to their promising potential in various fields such as optoelectronics,[1,2] sensing,[3,4] bioimaging[5,6] and light harvesting devices.[7] Key properties of these supramolecular ensembles, such as charge transport[8] or near infrared (NIR) emission,[9,10] are coupled to the molecule's arrangement in the assembled state. Accordingly, gaining control over intermolecular association, packing and morphology is a crucial step towards optimizing functional properties.[8,11] In this context, molecular design has become a powerful tool to tune (complex) energy landscapes in self-assembly, as evident by detailed analysis of a wide range of molecular building blocks.[12–38] While various studies have revealed that the intermolecular interactions encoded in the monomer design largely govern the self-assembly outcome, predicting these interactions by molecular design is far from easy. For example, we recently found that the functionalization of dye molecules with bulky substituents may unexpectedly stabilize H-type face-to-face stacking interactions despite the significant steric hindrance, contrary to conventional expectations based on literature.[39] Thus, there is still an urgent need for improved methods to predict structure–property relationships in self-assembly.

When considering the extensive literature on self-assembled π-conjugated systems, researchers often exploit the inherent planarity of π-conjugated scaffolds and dye molecules as a means to predictably control their stacking arrangements.[40,41] Although much less studied, non-planar π-conjugated molecules also demonstrate extended self-assembly potential in solution, given appropriate functionalization.[42–44] However, an unexplored aspect is whether the sole disruption of planarity in π-systems may originate multiple assembled states using the same building block. In this context, tetracoordinated organoboron dyes represent an ideal choice to investigate such effects, given that the typically used boron difluoride groups ($BF_2$) are arranged out of plane and, thus, may induce molecular distortions. In addition to the well-known boron dipyrromethene (BODIPY) dyes,[45–48] where the $BF_2$ is linked to a dipyrromethene core, various analogous scaffolds, including azaBODIPYs,[12] BODIHYs (hydrazones),[49,50] boron-locked anilido pyridines,[51] bis(borondifluoride)-8-imidazodipyrromethenes (BOIMPYs)[52]

*Universität Münster, Organisch-Chemisches Institut, Corrensstraße 36, Münster 48149, Germany. E-mail: fernandg@uni-muenster.de*

† Electronic supplementary information (ESI) available. See DOI: https://doi.org/10.1039/d4sc02499k

and azaBOIMPYs,[53] have been developed to leverage the photophysical properties and applications of this class of dyes. A particularly notable scaffold from the structural viewpoint is the BOPHY core (bis(difluoroboron)-1,2-bis((1*H*-pyrrol-2-yl) methylene)hydrazine), featuring two $BF_2$ groups within a tetracyclic pyrrole-boron difluoride structure.[54] Its structural resemblance to BODIPY, coupled with the non-planarity evident in its crystal structure,[54] renders it an ideal candidate for exploring the impact of planarity disruption on complex supramolecular polymerization.

In this work, we demonstrate that planarity breaking enables different supramolecular polymerization pathways with distinct molecular arrangements. To this end, we designed a new π-extended BOPHY dye containing amide groups and solubilizing alkyl side chains (**2**) and compared its supramolecular polymerization in non-polar media with that of a previously reported BODIPY analogue (**1**) with identical substituents (Scheme 1). Detailed spectroscopic investigations in methylcyclohexane (MCH) revealed that the BOPHY derivative (**2**) exists as either of two assembled states (**2A** & **2B**), unlike the BODIPY counterpart (**1**), which forms only one assembled state (**1A**).[39,55] Interestingly, both **2A** & **2B** are described by a cooperative mechanism, which is reflected in the formation of elongated fibres for both assembled states, as imaged by atomic force microscopy (AFM) and scanning electron microscopy (SEM). In contrast, despite following the same aggregation mechanism, the corresponding BODIPY derivative (**1**) forms much shorter one-dimensional (1D) assemblies than the BOPHY compound (**2**). This may result from the higher rigidity of the planar BODIPY core compared to the BOPHY counterpart, which limits extended hydrogen bonding formation. Nuclear magnetic resonance (NMR) and Fourier-transform infrared (FTIR) spectroscopy along with theoretical calculations disclose amide–amide hydrogen bonds of similar strength for both **2A** & **2B**. However, the key difference is the packing mode: while H-type antiparallel face-to-face stacking interactions are observed for kinetic assembly **2A**, the thermodynamic product **2B** is stabilized by a parallel slipped packing and concomitant ($BF_2$) F···H (*meso*) interactions. Therefore, the slightly non-planar structure of the BOPHY, together with the additional $BF_2$ group, allow for more diverse stacking possibilities compared to the planar BODIPY dye. These findings underline the importance of planarity breaking and out-of-plane substituents on chromophores as design elements in controlled supramolecular polymerization.

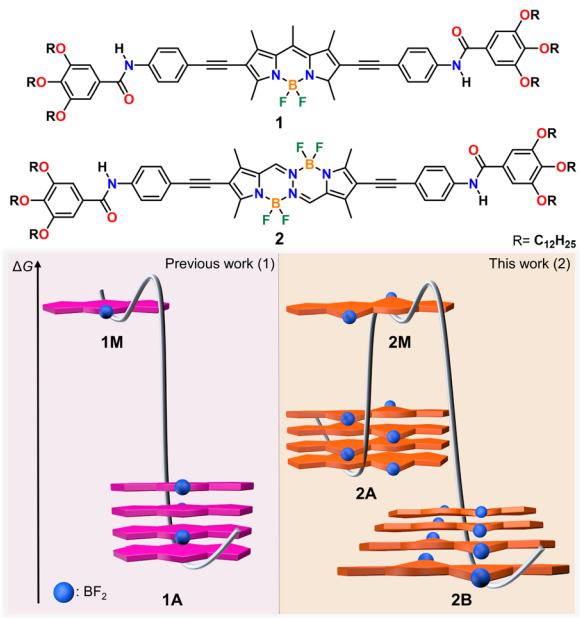


Scheme 1 Molecular structures of model compound BODIPY (**1**) and BOPHY dye (**2**) and cartoon representation of their molecular packing modes along with the energy profiles associated with their self-assembly.

## Results and discussion

### Synthesis and supramolecular polymerization

The target BOPHY derivative **2** was prepared following a synthetic procedure similar to that previously reported for the corresponding BODIPY derivative **1** (see ESI†).[55] The major synthetic step includes the carbon–carbon cross coupling Sonogashira reaction between the diiodo BOPHY derivative (**D**, Fig. S1†) and the alkyne side fragment functionalized with dodecyloxy chains (**E**, Fig. S1†), affording **2** with 39% yield (Fig. S1†).

The model BODIPY compound **1** has been thoroughly investigated in previous reports in terms of its supramolecular polymerization in non-polar solvents.[39,55] This derivative was found to self-associate in MCH into 1D H-type stacks (**1A**) as single thermodynamic product. Irrespective of the experimental conditions (stirring, sonication, thermal or solvophobic quenching, cooling/heating and denaturation), **1** forms exclusively this self-assembled state **1A** without traces of other kinetic products (Fig. 1a and b). Although **1A** is formed *via* the

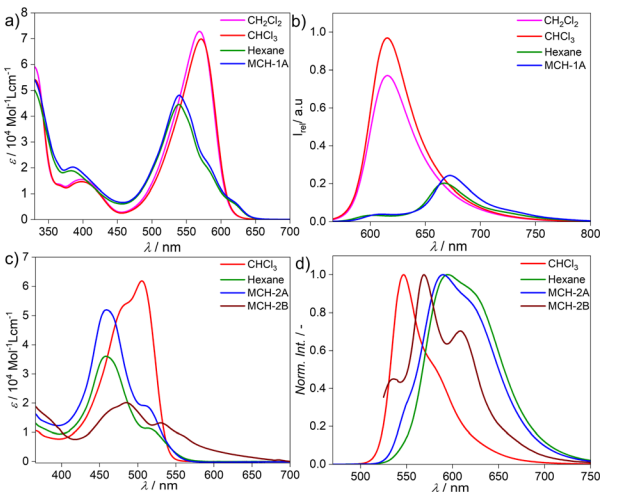


Fig. 1 Solvent-dependent absorption studies of: (a) compound **1**, (c) compound **2** and solvent-dependent fluorescence studies of: (b) compound **1**, $\lambda_{exc} = 510$ nm and (d) compound **2**, $\lambda_{exc} = 470$ nm at 298 K, $c = 2 \times 10^{-5}$ M.

cooperative mechanism, only short 1D assemblies are found in solution, which is attributed to increasing steric repulsion between the solubilizing chains hindering extended aggregate growth, as suggested by theoretical calculations.[56] We argue that the modification of the BODIPY core may be an effective strategy to tune this behaviour towards more feasible elongated growth. To probe this hypothesis, the photophysical properties of the BOPHY derivative (**2**) were first investigated using solvent-dependent absorption and emission spectroscopy (Fig. 1c and d). At a concentration of $2 \times 10^{-5}$ M, the absorption studies in moderately polar organic solvents like chloroform show spectral patterns that agree with a molecularly dissolved state (Fig. 1c), *i.e.* an absorption maximum at around 505 nm, corresponding to the $S_0 \rightarrow S_1$ transition of the BOPHY chromophore,[55] along with a shoulder at $\lambda_{max} = 482$ nm (Fig. 1c, see also Fig. S4a† for a comparison in multiple organic solvents). The corresponding photoluminescence studies of monomeric **2** in chloroform exhibit an emission maximum at ~546 nm along with a red shifted shoulder at 586 nm (Fig. 1d & S4b†). This trend changes considerably if the system is investigated in non-polar solvents, such as MCH, hexane, heptane or dodecane. In these media, a hypsochromic shift of the absorption maximum to 458 nm is observed with respect to the molecularly dissolved state ($\Delta\lambda = 50$ nm) (Fig. 1c & S4†). This self-assembled state will be termed from now on **2A**. In emission studies, **2A** is characterized by a sharp emission band at around 590 nm that is red-shifted compared to the molecularly dissolved state in chloroform ($\Delta\lambda = 44$ nm). The observed spectral features of **2A** bear close resemblance to those observed for **1** (**1A**), which are typical for a face-to-face (H-type) stacking of the BODIPY[55] as well as the BOPHY dyes.[57]

Variable temperature UV-vis studies (VT UV-vis) at different concentrations and cooling rates were subsequently recorded to gain insights into the self-assembly mechanism of the BOPHY derivative **2** in MCH. Upon cooling a solution of **2** from 363 K to 263 K with a ramp rate of 1 K $min^{-1}$, the absorption spectrum of the molecularly dissolved state (505 nm) shifts to lower wavelengths (458 nm), which can be attributed to the self-assembled species **2A** (Fig. 3a & S5†). The formation of **2A** was found to be independent of the cooling rate (Fig. S5†) and concentration (Fig. S6†), as also observed in VT emission studies (Fig. S7†), indicating that only one aggregate is obtained using thermal approaches. Plotting the degree of aggregation $\alpha_{agg}$ *vs.* the temperature from the heating and cooling experiments under similar conditions does not reveal any thermal hysteresis (Fig. S8†). This indicates that no kinetically trapped products are formed during the thermally-induced monomer-to-aggregate transition. To confirm this further, we subjected the sample to more drastic changes in the experimental conditions. Both solvophobic quenching (rapid injection of monomeric solution of **2** into an excess of MCH) as well as thermal quenching (fast cooling of a hot monomeric solution of **2** in MCH to 273 K) resulted in identical spectral features (Fig. S9a and b†), which are characteristic for the formation of aggregate **2A**. Hence, a single supramolecular species has been detected by thermal approaches, similar to what was found for the BODIPY counterpart **1**.[55]

However, dramatic differences in their time-dependent behaviour are witnessed for assemblies **1A** and **2A**. While **1A** remains invariant over time due to its thermodynamic stability,[55] **2A** forms over the course of one day at room temperature an energetically more favourable species (**2B**) (Fig. 2a). This transformation can be further accelerated using mechanical agitation in the form of sonication (10–20 seconds). The new self-assembled state **2B** is spectroscopically characterized by an absorption maximum centred at 484 nm (blue-shifted compared to the monomer) and a second, less intense red-shifted shoulder at 530 nm (Fig. 1c and 2a, brown spectrum). Spectral patterns with both H- and J-type characteristics, such as those of **2B**, are in line with the formation of HJ aggregates, as proposed in the literature.[58,59] The **2A** → **2B** transformation is accompanied by a colour change of the solution from yellow (**2A**) to light pink (**2B**) (inset of Fig. 2a). The new aggregated species (**2B**, $\phi_F = 12\%$) displays a lower photoluminescence quantum yield than **2A** ($\phi_F = 87\%$), which can be rationalized in different ways. The fluorescence found in aggregate **2A** might likely arise from the imperfect dye arrangement, possibly caused by a molecular scaffold that is not fully planar. Furthermore, we hypothesize that there could be a reduction in non-radiative decays due to the enhanced rigidity of the molecular chains in the π–π stacked aggregate.[60] The lower quantum yield of **2B** could be additionally explained by weakened excitonic coupling in the aggregated state compared to **2A**.[61]

To elucidate the nature of the **2A** → **2B** transformation (competitive or consecutive pathways), kinetic experiments at multiple concentrations were performed in MCH (10–40 μM) (Fig. 2a and b). As depicted in Fig. 2a, the spectral characteristics of **2A** are diminished over time as the spectral features of **2B** become dominant. Monitoring this transformation over time

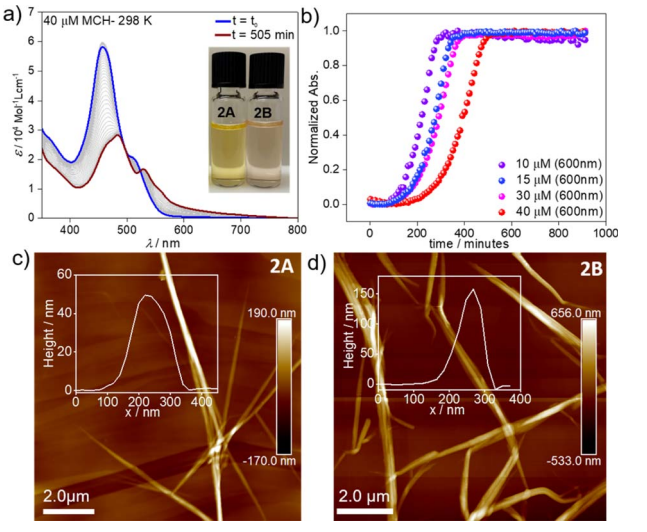


Fig. 2 (a) Time-dependent evolution of assembly **2A** into **2B** in MCH ($c = 4 \times 10^{-5}$ M) at 298 K. (b) Plot of absorbance *vs.* time at $\lambda = 600$ nm using different concentrations ($c = 10$–$40$ μM) at 298 K. AFM images of **2A** (c) and **2B** (d) obtained upon drop-casting the corresponding solutions ($c = 1 \times 10^{-5}$ M) on HOPG.

discloses a decelerated **2A** → **2B** conversion upon increasing the concentration, which indicates that both assembled states **2A** and **2B** are formed directly from the monomer, *i.e.* they are competitive (see energy diagram in Scheme 1 and Fig. 2b & S10†).

We next analysed the mechanism of formation of aggregates **2A** and **2B** by monitoring the absorption changes at a fixed wavelength against temperature during cooling experiments. In the case of aggregate **2A**, thermodynamic analysis of the experimental data obtained at different concentrations revealed a cooperative supramolecular polymerization process (Fig. 3a and e). Fitting these cooling curves (1 K $min^{-1}$) to the nucleation–elongation model[62] gave an average Gibbs free energy of $\Delta G = -35.20$ kJ $mol^{-1}$ (Tables 1 and S1†). On the other hand, as the assembly **2B** cannot be obtained by cooling experiments regardless of the cooling rate, we extracted the thermodynamic parameters from heating studies using a heating rate of 1 K $min^{-1}$. These experiments revealed that the absorption pattern of the molecularly dissolved state gradually rises at the expense of the absorption features of **2B** (Fig. 3b & S11†).

The corresponding heating curves *vs.* temperature obtained at $\lambda = 575$ nm also exhibited a non-sigmoidal shape, suggesting a cooperative mechanism for aggregate **2B.** Thermodynamic analysis of the plots at different concentrations (Fig. 3f) yielded a $\Delta G = -42.47$ kJ $mol^{-1}$ (Tables 1 and S2†). The lower $\Delta G$ value calculated for **2B** compared to **2A** demonstrates the superior stability of the former, which possibly arises from the more favourable chromophore packing arrangement. The high value of the nucleation penalty found for **2B** compared to **2A** suggests a higher cooperativity for the former (Tables S1 and S2†).[25]

Further information about the thermodynamic stability of the two assemblies was obtained by denaturation studies using $CHCl_3$ as a denaturing solvent while monitored by UV-vis spectroscopy. Addition of aliquots of monomeric **2** in $CHCl_3$ to the respective aggregate solutions of **2A** (Fig. 3c & S12†) or **2B** (Fig. 3d & S13†) at the same concentration leads to the disassembly of both aggregates directly to the monomeric species, further supporting the competitive nature of both pathways. Again, the cooperative model was employed to fit the denaturation measurements at different concentrations (Fig. 3g and h) for both aggregates.[63] The thermodynamic parameters extracted from this experiment agree with the results obtained from the VT experiments and point to a higher stability of **2B** ($\Delta G$ = −40.68 kJ $mol^{-1}$) compared to aggregate **2A** ($\Delta G$ = −35.40 kJ $mol^{-1}$) (Table S3†) under the investigated conditions. The obtained energy difference between the two assembled states lies within the range of systems to be considered supramolecular polymorphs (approximately 10 kJ $mol^{-1}$).[64–66,68]

Microscopy studies were performed to visualize the morphology of the assemblies after drop-casting their solutions onto highly oriented pyrolytic graphite (HOPG) or silicon wafer for AFM and SEM, respectively. Regardless of the employed

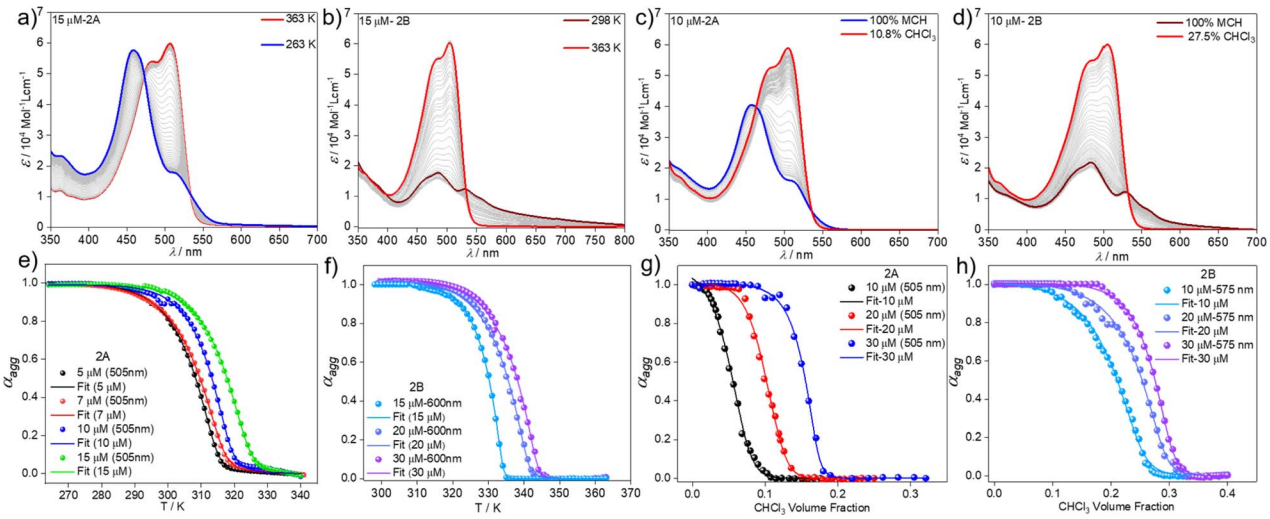


Fig. 3 VT UV-vis studies in MCH ($c = 1.5 \times 10^{-5}$ M) with a cooling/heating rate of 1 K $min^{-1}$ for **2A** (a) and **2B** (b). Plot of $\alpha_{agg}$ *vs.* temperature monitored at $\lambda = 505$ nm for **2A** (e) and at $\lambda = 600$ nm for **2B** (f) and corresponding fits to the nucleation–elongation model. UV-vis studies at different MCH–$CHCl_3$ ratios ($c = 1 \times 10^{-5}$ M) and 298 K for **2A** (c) and **2B** (d). Plot of $\alpha_{agg}$ *vs.* $CHCl_3$ volume fraction along with corresponding fits to the nucleation–elongation model for **2A** ($\lambda = 505$ nm) (g) and **2B** ($\lambda = 575$ nm) (h).

Table 1 Thermodynamic parameters obtained from VT UV-vis[62] and denaturation experiments[63] for aggregates **2A** and **2B** along with hydrogen bond distances calculated from theoretical calculations

| Aggregate | $\Delta G_0$ (kJ $mol^{-1}$) VT | $\Delta G_0$ (kJ $mol^{-1}$) denaturation | C–H···F–B distances (Å) | N–H···O=C distances (Å) |
|---|---|---|---|---|
| **2A** | −35.20 | −35.40 | 2.468, 3.595 | 2.105, 2.263 |
| **2B** | −42.47 | −40.68 | 1.999, 1.967 | 1.992, 2.074 |

substrate, the structures could be visualized as bundles of highly elongated fibre-like structures. AFM images of aggregate **2A** showed the formation of needle-like morphologies with a height of *ca.* 50 nm and *ca.* 5–7 μm in length (Fig. 2c). In the case of **2B**, elongated fibres can also be observed but with a height of approximately 150 nm and a length of *ca.* 3–5 μm (Fig. 2d). We infer from these results that both assemblies are significantly stabilized by hierarchical effects, leading to an efficient bundling of the structures.[67,69] In the case of **2B**, this behaviour is particularly pronounced (as evident from the increase in the height of the fibre bundles). We argue that this change in hierarchical interactions is driven by a decrease in the density of the solubilizing alkyl shell (*vide infra*), which allows the chains of neighbouring stacks to interdigitate more effectively in **2B**. These observations are consistent with previous reports, which found an increased tendency to form hierarchical structures as a consequence of increased flexibility of solubilizing alkyl chains.[68] In addition, polymerization processes driven by solvent–solute interactions have been demonstrated to follow a similar mechanism.[69,70] The corresponding SEM studies (Fig. S18 & S19†) agree with the above-mentioned results extracted from the AFM analysis, revealing less bundled fibres for **2A** (Fig. S20†) and more clustered fibres for **2B** (Fig. S21†) on the silicon wafer surface. TEM analysis (Fig. S22†) also reproduce the results from AFM and SEM.

In order to rationalize the differences in molecular packing, FTIR measurements as well as $^1$H NMR studies were performed. For molecularly dissolved **2** in $CHCl_3$ at 1 mM (Fig. S16†), we found N–H and C=O stretching bands at $\nu_{N-H} = 3432$ cm$^{-1}$ and $\nu_{C=O} = 1673$ cm$^{-1}$, respectively. The FTIR spectrum of aggregate **2A** (1 mM in MCH, Fig. S17†) revealed the shifting of these bands to $\nu_{N-H} = 3278$ cm$^{-1}$ and $\nu_{C=O} = 1646$ cm$^{-1}$, indicating the existence of N–H···O=C hydrogen bonds. In the case of aggregate **2B** (1 mM in MCH, Fig. S17†), a slightly lower value for the N–H stretching ($\nu_{N-H} = 3259$ cm$^{-1}$) was observed, while the C=O stretching band showed a similar frequency ($\nu_{C=O} = 1646$ cm$^{-1}$) when compared to **2A**. The slightly lower value of the N–H stretching frequency band indicates the marginally stronger amide hydrogen bonding interactions for the thermodynamic product **2B**,[71] while the identical C=O frequencies might suggest the existence of defects in **2B**. To further analyse the differences in packing of aggregates **2A** and **2B**, we performed 2D $^1$H–$^{19}$F NMR spectroscopy ($^1$H–$^{19}$F HOESY NMR). We simultaneously monitored the 2D $^1$H–$^{19}$F HOESY NMR spectra of **2A** (70% MCH-$d_{14}$ + 30% $CDCl_3$) and **2B** (90% MCH-$d_{14}$ + 10% $CDCl_3$) at 328 K ($c = 5$ mM) (Fig. 4a, c & S15†). Both aggregates revealed a strong correlation signal that corresponds to intermolecular interactions between the *meso*-hydrogens of the BOPHY core and the fluorine atoms connected to the boron. Additionally, both assemblies revealed a correlation between the methyl protons on the BOPHY core and the fluorine atoms, suggesting similar stabilizing interactions in both aggregates **2A** and **2B**, albeit with slightly different arrangements of the chromophores (Fig. 4a, c, S29 & S30†). Based on the similar 2D HOESY NMR experiment, we assume that both aggregates **2A** and **2B** may adopt a packing that maintains both types of hydrogen bonding interactions depending upon the feasible alignment of the BOPHY chromophore (parallel or antiparallel).

## Theoretical studies

To gain further insights on the packing modes of the aggregates, theoretical calculations—DFT, (B3LYP/6-31(+)G(d,p))[72,73]—were performed on monomers, dimers and trimers of **2A** and **2B**. In order to reduce the computational costs during the DFT calculations, we replaced the dodecyloxy side chains with methoxy groups. To corroborate the validity of our optimized structure, we calculated the absorption spectra for the monomers and trimers (rcam-B3LYP/6–31(+)G(d,p))[72,73] and compared them with the experimental ones (Fig. 5c, d & S24†). The calculated absorption spectrum of a trimer of aggregate **2A** shows a blue shift with respect to the monomeric species, which validates the proposed packing on the basis of the experimental data (Fig. 5a and c). The BOPHY chromophores within the trimer of **2A** are arranged in a face-to-face antiparallel fashion, stabilized through N–H···OC hydrogen bonds as well as by weak interactions between the *meso*-hydrogens and the fluorines on the BOPHY core (Fig. 4b and 5a). Similarly, a trimer of **2B** was optimized. The proposed packing displays the chromophores in a parallel arrangement, with the fluorine atoms of each BOPHY unit in the stack pointing in the same direction (Fig. 4d and 5b).

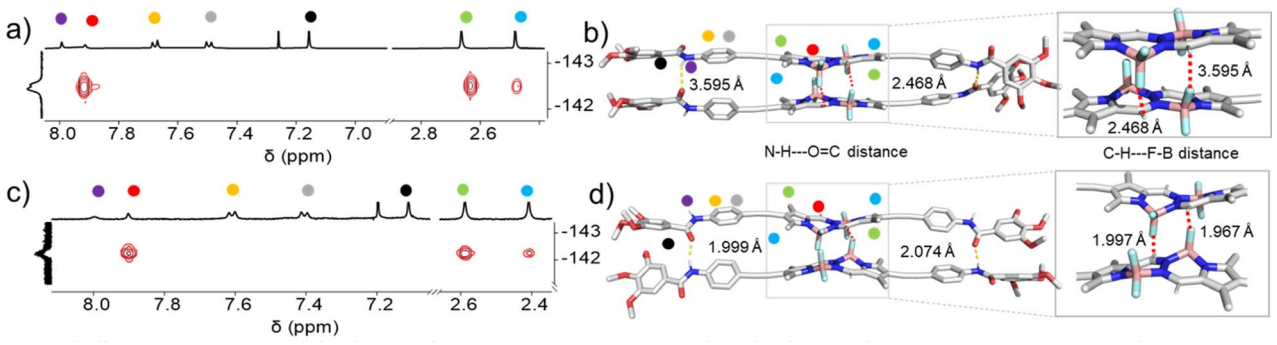


Fig. 4 $^1$H–$^{19}$F HOESY 2D NMR studies of (a) **2A** ($c = 5 \times 10^{-3}$ M, 70% MCH-$d_{14}$ + 30% $CDCl_3$ at 323 K) and (c) **2B** ($c = 5 \times 10^{-3}$ M, 90% MCH-$d_{14}$ + 10% $CDCl_3$ at 323 K) illustrating the interactions of the *meso*-hydrogens of the BOPHY with the fluorine atoms. Corresponding molecular packing governed by amide–amide hydrogen bonding interactions as well as unconventional interactions between the *meso*-hydrogens and fluorines of the difluoride groups illustrated in (b) **2A** and (d) **2B**. The respective protons are also marked in the figure.

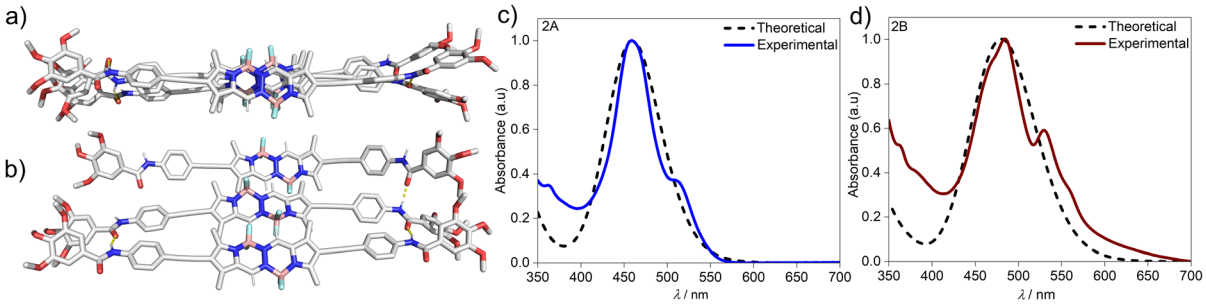


Fig. 5 Geometry-optimized trimer structures of (a) aggregate **2A** and (b) aggregate **2B** obtained by DFT calculations (B3LYP/6-31(+)G(d,p)) and corresponding rCAM-B3LYP/6-31g(d,p) optimized absorption spectra of trimers of (c) **2A** and (d) **2B**.

Arranging the chromophores in a face-to-face fashion, as it was the case for the antiparallel packing of **2A**, is not possible due to the steric hindrance of the out-of-plane fluorine atoms. As a result, the monomers are required to shift laterally along the short axis, retaining the amide N–H···OC hydrogen bonds as well the interactions between the *meso*-hydrogen of the core with the fluorines of the neighbouring molecule, as experimentally observed (Fig. 5b and d). The N–H···O=C amide hydrogen bond distances found for aggregate **2B** (≈1.9–2.0 Å) are shorter than those of **2A** (≈2.1–2.2 Å), suggestive of comparatively stronger hydrogen bonding interactions in the former aggregate (**2B**) (Table 1 & Fig. 4). These results agree with the FTIR measurements of both aggregates (Fig. S17†). Similarly, the C–H···F–B hydrogen bonding distance of aggregate **2A** (≈2.4–3.5 Å) was also found to be greater than that of **2B** (≈2.0 Å) (Table 1 & Fig. 4), again indicating comparatively stronger interactions within **2B**. The predicted absorption spectra obtained for this trimer stack is in good agreement with the experimental trends (Fig. 5c and d). Thus, these studies suggest that the pathway complexity in the self-assembly of BOPHY derivative **2** arises from the different packing possibilities of the BOPHY chromophores due to the oppositely oriented $BF_2$ groups, resulting in a loss of planarity.

## Conclusions

In summary, we have elucidated the supramolecular polymerization of a new class of chromophore (BOPHY), which is structurally analogous to the well-known BODIPY core, but it features an additional fused heterocycle and two oppositely oriented $BF_2$ groups instead of one. These structural differences are responsible for the slight loss of planarity for the BOPHY core compared to the BODIPY counterpart, which greatly affects the overall supramolecular self-assembly. While the model BODIPY derivative **1** exists as only one type of supramolecular structure in non-polar media with face-to face (H-type) molecular packing, the new BOPHY derivative **2** forms two competitive supramolecular polymers. This can be explained by the additional $BF_2$ unit of the BOPHY derivative, which affects the symmetry, sterics and planarity of the system, thereby enabling different packing possibilities and promoting pathway complexity. Initially, BOPHY **2** forms a kinetically controlled H-type supramolecular polymer (**2A**) in MCH that evolves over time into the thermodynamic product (**2B**) *via* a competitive pathway. According to the theoretical results, the $BF_2$ groups build steric hindrance within the antiparallel H-type face-to-face stacks **2A**, forcing the aggregates to rearrange into a more stable supramolecular polymer **2B** with laterally displaced monomer units. This arrangement not only minimizes the steric hindrance but it also maintains the hydrogen bonds between the amide side groups, which were experimentally found to be stronger for the thermodynamic assembly (**2B**). Interestingly, this pathway complexity is absent in the case of the BODIPY derivative **1**, since the H-type antiparallel dye arrangement is highly efficient due to the alternated, antiparallel orientation of the single, $BF_2$ unit per monomer. We conclude that the main additional structural component of the BOPHY chromophore, *i.e.* the two $BF_2$ groups, break the planarity of the π-system and enable different types of stacking interactions due to altered sterics and symmetry. This study highlights the versatility of the novel BOPHY chromophore in supramolecular self-assembly and introduces the break in planarity as a new molecular design strategy in controlled supramolecular polymerization.

## Data availability

All the experimental data have been shown in the ESI.†

## Author contributions

Rasitha Manha Veedu: synthesis, investigation, methodology, writing – original draft (lead). Zulema Fernández: theoretical calculations, writing – original draft (support). Nils Bäumer: AFM measurements, writing – review and editing. Antonia Albers: TEM measurements. Gustavo Fernández: conceptualization, writing – review and editing, supervision and funding acquisition.

## Conflicts of interest

There are no conflicts to declare.

## Acknowledgements

We thank the the Deutsche Forschungsgemeinschaft (DFG, German Research Foundation) [SFB 858 (R. M. V.), SFB 1450 inSight—431460824, project B01 (R. M. V. and A. A.) and GRK

2678 – 437785492 (N. B.)] for financial support. Z. F. gratefully acknowledges the Alexander von Humboldt foundation for funding.

## Notes and references

1 S. Ghosh, V. K. Praveen and A. Ajayaghosh, *Annu. Rev. Mater. Res.*, 2016, **46**, 235–262.
2 S. S. Babu, V. K. Praveen and A. Ajayaghosh, *Chem. Rev.*, 2014, **114**, 1973–2129.
3 D. Cao, Z. Liu, P. Verwilst, S. Koo, P. Jangjili, J. S. Kim and W. Lin, *Chem. Rev.*, 2019, **119**, 10403–10519.
4 K. S, B. Sam, L. George, S. Y. N and A. Varghese, *J. Fluoresc.*, 2021, **31**, 1251–1276.
5 Q. Yang, X. Chang, J. Y. Lee, T. R. Olivera, M. Saji, H. Wisniewski, S. Kim and F. Zhang, *ACS Appl. Bio Mater.*, 2022, **5**, 4652–4667.
6 J. Tian, F. Lin, S.-B. Yu, J. Yu, Q. Tang and Z.-T. Li, *Aggregate*, 2022, **3**, e187.
7 S. R. Trenor, A. R. Shultz, B. J. Love and T. E. Long, *Chem. Rev.*, 2004, **104**, 3059–3077.
8 K. Sakakibara, P. Chithra, B. Das, T. Mori, M. Akada, J. Labuta, T. Tsuruoka, S. Maji, S. Furumi, L. K. Shrestha, J. P. Hill, S. Acharya, K. Ariga and A. Ajayaghosh, *J. Am. Chem. Soc.*, 2014, **136**, 8548–8551.
9 K. Li, X. Duan, Z. Jiang, D. Ding, Y. Chen, G.-Q. Zhang and Z. Liu, *Nat. Commun.*, 2021, **12**, 2376.
10 Z. Chen and Z. Chen, *Org. Chem. Front.*, 2023, **10**, 2581–2602.
11 A. Isobe, T. Kajitani and S. Yagai, *Angew. Chem., Int. Ed.*, 2023, **62**, e202312516.
12 H. Choi, S. Ogi, N. Ando and S. Yamaguchi, *J. Am. Chem. Soc.*, 2023, **143**, 2953–2961.
13 J.-K. Kim, E. Lee, M.-C. Kim, E. Sim and M. Lee, *J. Am. Chem. Soc.*, 2009, **131**, 17768–17770.
14 I. Helmers, B. Shen, K. K. Kartha, R. Q. Albuquerque, M. Lee and G. Fernández, *Angew. Chem., Int. Ed.*, 2020, **59**, 5675–5682.
15 S. Ogi, T. Fukui, M. L. Jue, M. Takeuchi and K. Sugiyasu, *Angew. Chem., Int. Ed.*, 2014, **53**, 14363–14367.
16 S. Ogi, V. Stepanenko, J. Thein and F. Würthner, *J. Am. Chem. Soc.*, 2016, **138**, 670–678.
17 M. H.-Y. Chan and V. W.-W. Yam, *J. Am. Chem. Soc.*, 2022, **144**, 22805–22825.
18 N. Sasaki, M. F. J. Mabesoone, J. Kikkawa, T. Fukui, N. Shioya, T. Shimoaka, T. Hasegawa, H. Takagi, R. Haruki, N. Shimizu, S. Adachi, E. W. Meijer, M. Takeuchi and K. Sugiyasu, *Nat. Commun.*, 2020, **11**, 3578.
19 C. Naranjo, S. Adalid, R. Gómez and L. Sánchez, *Angew. Chem., Int. Ed.*, 2023, **62**, e202218572.
20 M. A. Martínez, A. Doncel-Giménez, J. Cerdá, J. Calbo, R. Rodríguez, J. Aragó, J. Crassous, E. Ortí and L. Sánchez, *J. Am. Chem. Soc.*, 2021, **143**, 13281–13291.
21 Y. Han, Z. Gao, C. Wang, R. Zhong and F. Wang, *Coord. Chem. Rev.*, 2020, **414**, 213300.
22 G. Ghosh, *Giant*, 2023, **14**, 100160.
23 M. U. Lone, N. Sahu, R. K. Roy and B. Adhikari, *Chem.–Eur. J.*, 2023, **29**, e202202711.
24 F. Wang, R. Liao and F. Wang, *Angew. Chem., Int. Ed.*, 2023, **62**, e202305827.
25 C. Kulkarni, E. W. Meijer and A. R. A. Palmans, *Acc. Chem. Res.*, 2017, **50**, 1928–1936.
26 T. Aida and E. W. Meijer, *Isr. J. Chem.*, 2020, **60**, 33–47.
27 S. V. Bhosale, M. Al Kobaisi, R. W. Jadhav, P. P. Morajkar, L. A. Jones and S. George, *Chem. Soc. Rev.*, 2021, **50**, 9845–9998.
28 S. Sarkar, R. Laishram, D. Deb and S. J. George, *J. Am. Chem. Soc.*, 2023, **145**, 22009–22018.
29 G. Das, A. Anand, B. Vedhanarayanan, A. Padmakumar, V. K. Praveen and A. Ajayaghosh, *Chem.–Eur. J.*, 2023, **29**, e202301819.
30 P. Khanra, A. K. Singh, L. Roy and A. Das, *J. Am. Chem. Soc.*, 2023, **145**, 5270–5284.
31 V. Vázquez-González, M. J. Mayoral, F. Aparicio, P. Martínez-Arjona and D. González-Rodríguez, *ChemPlusChem*, 2021, **86**, 1087–1109.
32 Q. Wang, W.-P. To, X. Chang and C.-M. Che, *Chem*, 2020, **6**, 945–967.
33 S. Barman, A. Pal, A. Mukherjee, S. Paul, A. Datta and S. Ghosh, *Chem.–Eur. J.*, 2024, **30**, e20230312.
34 S. Yagai, Y. Kitamoto, S. Datta and B. Adhikari, *Acc. Chem. Res.*, 2019, **52**, 1325–1335.
35 F. García, R. Gómez and L. Sánchez, *Chem. Soc. Rev.*, 2023, **52**, 7524–7548.
36 M. Wehner and F. Würthner, *Nat. Rev. Chem*, 2020, **4**, 38–53.
37 J. Matern, Y. Dorca, L. Sánchez and G. Fernández, *Angew. Chem., Int. Ed.*, 2019, **58**, 16730–16740.
38 G. Ghosh, P. Dey and S. Ghosh, *Chem. Commun.*, 2020, **56**, 6757–6769.
39 R. Manha Veedu, N. Niemeyer, N. Bäumer, K. Kartha Kalathil, J. Neugebauer and G. Fernández, *Angew. Chem., Int. Ed.*, 2023, e202314211.
40 Z. Chen, A. Lohr, C. R. Saha-Möller and F. Würthner, *Chem. Soc. Rev.*, 2009, **38**, 564–584.
41 Z. Fernández, L. Sánchez, S. S. Babu and G. Fernández, *Angew. Chem., Int. Ed.*, 2024, e202402259.
42 V. Grande, B. Soberats, S. Herbst, V. Stepanenko and F. Würthner, *Chem. Sci.*, 2018, **9**, 6904–6911.
43 M. J. Mayoral, J. Guilleme, J. Calbo, J. Aragó, F. Aparicio, E. Ortí, T. Torres and D. González-Rodríguez, *J. Am. Chem. Soc.*, 2020, **142**, 21017–21031.
44 R. Rodríguez, C. Naranjo, A. Kumar, P. Matozzo, T. K. Das, Q. Zhu, N. Vanthuyne, R. Gómez, R. Naaman, L. Sánchez and J. Crassous, *J. Am. Chem. Soc.*, 2022, **144**, 7709–7719.
45 S. Cherumukkil, B. Vedhanarayanan, G. Das, V. K. Praveen and A. Ajayaghosh, *Bull. Chem. Soc. Jpn.*, 2018, **91**, 100–120.
46 B. Matarranz and G. Fernández, *Chem. Phys. Rev.*, 2021, **2**, 041304.
47 Y. Zhang, S. Yuan, P. Liu, L. Jing, H. Pan, X.-K. Ren and Z. Chen, *Org. Chem. Front.*, 2021, **8**, 4078–4085.
48 J. Ding, H. Pan, H. Wang, X.-K. Ren and Z. Chen, *Org. Chem. Front.*, 2022, **9**, 3949–3955.
49 Y. Yang, X. Su, C. N. Carroll and I. Aprahamian, *Chem. Sci.*, 2012, **3**, 610–613.

50 H. Qian, M. E. Cousins, E. H. Horak, A. Wakefield, M. D. Liptak and I. Aprahamian, *Nat. Chem.*, 2017, **9**, 83–87.
51 J. F. Araneda, W. E. Piers, B. Heyne, M. Parvez and R. McDonald, *Angew. Chem., Int. Ed.*, 2011, **50**, 12214–12217.
52 L. J. Patalag, P. G. Jones and D. B. Werz, *Angew. Chem., Int. Ed.*, 2016, **55**, 13340–13344.
53 L. J. Patalag, P. G. Jones and D. B. Werz, *Chem.–Eur. J.*, 2017, **23**, 15903–15907.
54 I.-S. Tamgho, A. Hasheminasab, J. T. Engle, V. N. Nemykin and C. J. Ziegler, *J. Am. Chem. Soc.*, 2014, **136**, 5623–5626.
55 A. Rödle, B. Ritschel, C. Mück-Lichtenfeld, V. Stepanenko and G. Fernández, *Chem.–Eur. J.*, 2016, **22**, 15772–15777.
56 Y. Dorca, C. Naranjo, G. Ghosh, B. Soberats, J. Calbo, E. Ortí, G. Fernández and L. Sánchez, *Chem. Sci.*, 2021, **13**, 81–89.
57 L. Jiang, H. Gao, L. Gai and Z. Shen, *New J. Chem.*, 2018, **42**, 8271–8275.
58 H. Yamagata, D. S. Maxwell, J. Fan, K. R. Kittilstved, A. L. Briseno, M. D. Barnes and F. C. Spano, *J. Phys. Chem. C*, 2014, **49**, 28842–28854.
59 N. J. Hestand and F. C. Spano, *Acc. Chem. Res.*, 2017, **50**, 341–350.
60 S. Chakraborty, P. Debnath, D. Dey, D. Bhattacharjee and S. A. Hussain, *J. Photochem. Photobiol., A*, 2014, **293**, 57–64.
61 I. Helmers, M. Niehues, K. K. Kartha, B. J. Ravoo and G. Fernández, *Chem. Commun.*, 2020, **56**, 8944–8947.
62 H. M. M. Eikelder, A. J. Markvoort, T. F. A. de Greef and P. A. J. Hilbers, *J. Phys. Chem. B*, 2012, **116**, 5291–5301.
63 P. A. Korevaar, C. Schaefer, T. F. A. de Greef and E. W. Meijer, *J. Am. Chem. Soc.*, 2012, **134**, 13482–13491.
64 M. Wehner, M. I. S. Röhr, M. Bühler, V. Stepanenko, W. Wagner and F. Würthner, *J. Am. Chem. Soc.*, 2019, **141**, 6092–6107.
65 L. Rubert, M. F. Islam, A. B. Greytak, R. Prakash, M. D. Smith, R. M. Gomila, A. Frontera, L. S. Shimizu and B. Soberats, *Angew. Chem., Int. Ed.*, 2023, **62**, e202312223.
66 S. Bujosa, A. Doncel-Giménez, N. Bäumer, G. Fernández, E. Ortí, A. Costa, C. Rotger, J. Aragó and B. Soberats, *Angew. Chem., Int. Ed.*, 2022, **61**, e202213345.
67 N. Bäumer, E. Castellanos, B. Soberats and G. Fernández, *Nat. Commun.*, 2023, **14**, 1084.
68 J. Matern, N. Bäumer and G. Fernández, *J. Am. Chem. Soc.*, 2021, **143**(18), 7164–7175.
69 C. Kulkarni, P. A. Korevaar, K. K. Bejagam, A. R. A. Palmans, E. W. Meijer and S. J. George, *J. Am. Chem. Soc.*, 2017, **139**, 13867–13875.
70 G. Ghosh, A. Chakraborty, P. Pal, B. Jana and S. Ghosh, *Chem.–Eur. J.*, 2022, **28**, e202201082.
71 A. Langenstroer, K. K. Kartha, Y. Dorca, J. Droste, V. Stepanenko, R. Q. Albuquerque, M. R. Hansen, L. Sánchez and G. Fernández, *J. Am. Chem. Soc.*, 2019, **141**, 5192–5200.
72 A. D. Becke, *J. Chem. Phys.*, 1993, **98**, 5648–5652.
73 M. M. Francl, W. J. Pietro, W. J. Hehre, J. S. Binkley, M. S. Gordon, D. J. DeFrees and J. A. Pople, *J. Chem. Phys.*, 1982, **77**, 3654–3665.